95 GHz Indoor Propagation Measurement and Statistically Enhanced 3GPP Channel Model for Sub-THz Indoor Short-Range Communications

Yusuke Koda[1], Norichika Ohmi[1], Hiroaki Endo[1], and Hiroshi Harada[1]

[1]Graduate School of Informatics, Kyoto University

August 06, 2024

Abstract

This study presents a 95 GHz indoor channel measurement campaign for a short-range communication scenario and proposes an improved intra-cluster stochastic channel generation procedure compatible with the well-known 3GPP stochastic channel model (SCM). The current 3GPP SCM casts itself to apply to the frequency range up to 100 GHz; however, there is no measurement-based validation for this upper limit because of the lack of measurement campaign for 90 GHz–100 GHz. Moreover, the 3GPP SCM generates the characteristics of intra-cluster subpath parameters equally to all clusters in terms of the number of clusters and per-cluster delay spread, falling short of capturing real channel characteristics, particularly for the usage of large bandwidth. Motivated by the first limitation, we holistically derive the statistical parameters of the 95 GHz channel propagation characteristics in a simple conference room scenario and compare these parameters with our 60 GHz channel measurement results in a similar environment. This investigation confirms the feasibility of the 60 GHz statistical parameters generalized for the 95 GHz band at least in the measured scenario. Moreover, to solve the second issue, we propose an unequal intra-cluster subpath generation procedure, serving as a 3GPPcompatible amendment for accurate channel generation. Numerical evaluation reveals the feasibility of generating channel impulse responses capturing more accurate intra-cluster subpath characteristics than the current 3GPP SCM.

IEEE Journal of Microwaves

Received Day Month 20XX; revised Day Month 20XX; accepted Day Month 20XX; date of current version Day Month 20XX.

Digital Object Identifier 10.1109/JMW.20XX.0000000

95 GHz Indoor Propagation Measurement and Statistically-Enhanced 3GPP Channel Model for Sub-THz Indoor Short-Range Communications

Yusuke Koda, Member, IEEE, Norichika Ohmi, Non-Member, IEEE
Hiroaki Endo, Student Member, IEEE, and Hiroshi Harada, Senior Member, IEEE

Graduate School of Informatics, Kyoto University, Sakyo-ku Yoshida-Honmachi, Kyoto, Japan

CORRESPONDING AUTHOR: Yusuke Koda (e-mail: koda@i.kyoto-u.ac.jp).

These results were partly obtained from the commissioned research (No. JPJ012368C04201) by the National Institute of Information and Communications Technology (NICT), Japan. A part of this research is also supported by the Ministry of Internal Affairs and Communications in Japan (SCOPE #JPJ00595)

An earlier version [1] of this paper was submitted and accepted in part to the 2024 Annual IEEE Wireless Communications and Networking Conference (IEEE WCNC 2024), Dubai, United Arab Emirates.

ABSTRACT This study presents a 95 GHz indoor channel measurement campaign for a short-range communication scenario and proposes an improved intra-cluster stochastic channel generation procedure compatible with the well-known 3GPP stochastic channel model (SCM). The current 3GPP SCM casts itself to apply to the frequency range up to 100 GHz; however, there is no measurement-based validation for this upper limit because of the lack of measurement campaign for 90 GHz–100 GHz. Moreover, the 3GPP SCM generates the characteristics of intra-cluster subpath parameters equally to all clusters in terms of the number of clusters and per-cluster delay spread, falling short of capturing real channel characteristics, particularly for the usage of large bandwidth. Motivated by the first limitation, we holistically derive the statistical parameters of the 95 GHz channel propagation characteristics in a simple conference room scenario and compare these parameters with our 60 GHz channel measurement results in a similar environment. This investigation confirms the feasibility of the 60 GHz statistical parameters generalized for the 95 GHz band at least in the measured scenario. Moreover, to solve the second issue, we propose an unequal intra-cluster subpath generation procedure, serving as a 3GPP-compatible amendment for accurate channel generation. Numerical evaluation reveals the feasibility of generating channel impulse responses capturing more accurate intra-cluster subpath characteristics than the current 3GPP SCM.

INDEX TERMS 95 GHz, Propagation measurement, Channel model, Indoor short-range, 3GPP SCM

I. INTRODUCTION

As the fifth-generation and sixth-generation mobile networks are expected to provide a platform for operating distributed and autonomous systems, substantial demand for extremely high-rate and low-latency wireless communications will arise [2]. To meet such demand, the usage of the millimeter wave (mmWave) and sub-terahertz (sub-THz) spectrum has attracted considerable attention [3, 4]. This is supported by the fact that the spectrum spanning 30 GHz–300 GHz provides an abundant bandwidth for wireless communications, and extremely high-rate and even low-latency communication can be performed in theory. Hence, designing wireless communication systems operating in the mmWave bands is an area of interest for next-generation wireless communication systems.

To design wireless communication systems operating at this band, a stochastic channel model (SCM) is required, and the third-generation partnership project (3GPP) SCM is one of the world's standard models for the mmWave band

up to 100 GHz [5]. In the technical report (TR) 38.901 [5] explaining the 3GPP SCM, a set of statistical parameters and a multipath channel impulse response (CIR) generation procedure are holistically reported for urban micro (UMi), urban macro (UMa), indoor hotspot (InH), and indoor factory (InF) environments. These generated CIRs can be immediately used for link-level simulation (e.g., 60 GHz simulations in [6]), based on which designed waveforms for upcoming mmWave communication systems are evaluated and discussed. Outside the 3GPP, 3GPP SCM-based mmWave channel models have also been developed in an academic large-scale European project [7] and other measurement campaigns in the InH office at 60 GHz [8] and 100 GHz [9, 10]. Moreover, open-source software is also developed in [11] based on the 3GPP SCM. In these senses, the 3GPP SCM has been a foundation driving the development of mmWave wireless communication systems.

Notably, the 3GPP SCM applies to not only the aforementioned infrastructure-type scenarios, such as UMi, UMa, InH, and InF but also shorter-range device-to-device communication scenarios, such as wireless personal area network (WPAN) and vehicular-to-vehicular (V2V) communication scenarios. The reason behind this applicability is that the generated CIR for mmWave communications shares a common basic structure that consists of inter-cluster and intra-cluster parameters [12]. In [13], a concrete amendment of the 3GPP SCM-based channel generation framework for mmWave WPAN scenarios was provided using real-world propagation measurements and showed consistent performance with the precedented 60 GHz WPAN channel model [14]. For V2V communications, the 3GPP published a new TR indexed 37.885 based on the 3GPP SCM [15], which applies to the 60 GHz band. Hence, the 3GPP SCM exhibits a huge potential to become a unified and general platform to test mmWave communication systems for various scenarios and use cases.

Thus, the following demanding question arises: *whether and to what extent the 3GPP SCM and reported statistical parameters apply to the band around 100 GHz (i.e., lower sub-THz band) with a larger bandwidth use-case*. Indeed, we can hypothesize that the band around 100 GHz retains similar propagation characteristics to the extensively studied 28 GHz/60 GHz bands. This fact may be the reason for the 3GPP SCM stating itself to be applicable up to 100 GHz. However, there are few measurement-based studies at this band, meaning that the aforementioned hypothesis about 100 GHz propagation characteristics has not fully been confirmed.

In more detail, to shed light on the hypothesis, a holistic comparison between 28 GHz/60 GHz and 100 GHz in the large-scale parameters (LSPs), i.e., statistical parameters dictating multipath clusters, in the format of the 3GPP SCM parameter table is required. However, to the best of our knowledge, there are no such comparative studies, which can be regarded as the limitation of the previous works. For example, Li et.al. conducted a multipath propagation in an indoor office [9] at around 100 GHz, and Chang et. al. conducted similar measurements in the same office and outdoor environments [10] at the same band. However, these studies did not provide any comparative measurements with the 28 GHz/60 GHz band in the same environment. In [16], a 105 GHz measurement was performed in a factory environment while suffering from the same issues as [9, 10]. Liu et. al. conducted a comparative measurement among 6 GHz, 26 GHz, and 105 GHz and provided several LSPs such as delay spread and K-factor [17]. However, the focus of this work was on the channel sparsity analysis, and several LSPs (e.g., angular spread, delay scaling factor, and per-cluster shadow fading term) were not reported. In the authors' previous works [18, 19], 105 GHz channel measurement was performed in several office environments and compared with the 60 GHz in the same environment. However, as in [17], several LSPs are missing, meaning that no comprehensive comparisons in LSPs were performed. Inomata et. al. provided a comparative propagation measurement at 26.4 GHz, 66.5 GHz, and 97.5 GHz in [20, 21]; however, the focus of these studies was on the electromagnetic characteristics, not on statistical characteristics of multipath arrivals. In [22]–[24], a 94 GHz propagation measurement in a body area network was performed; however, these were not a field measurement where the 3GPP-like multipath characterization was not conducted. To summarize, there are no studies on a holistic comparison between 28 GHz/60 GHz and 100 GHz in terms of LSPs filling the 3GPP SCM parameter table.

Motivated by this issue, this study first conducts a wideband 95 GHz multipath propagation measurement in a similar environment conducted in [13] at 60 GHz for a WPAN-like indoor short-range use case. Based on these measurement results, we holistically derive large-scale parameters (LSPs) in the 3GPP SCM, i.e., statistical parameters, such as delay spread, angular spread, K-factor, and their correlations, and compare them with the parameters measured in 60 GHz WPAN scenarios [13]. This comparison yields insight into the fewer distinctions between these two bands in the statistical channel parameters, shedding light on the hypothesis that common LSP values are used for both the 60 GHz band and the band around 100 GHz.

Regarding the aforementioned question, besides the 100 GHz propagation characteristics, it is also questionable whether the 3GPP SCM is applicable for the “larger bandwidth use-case.” in terms of the small-scale intra-cluster characteristics. For the 100 GHz and more, the usage of a large bandwidth in the order of giga-hertz is expected; hence, an accurate modeling of intra-cluster rays is essential. However, the 3GPP SCM generates the equal number of intra-cluster rays in the equal intra-cluster delay and angular spreads for all clusters, and this equal intra-cluster ray production is not necessarily accurate as found from our measurement results. Hence, an amendment for this channel generation procedure suited for a large bandwidth use case is required.

Hence, motivated by the issue, we propose a simple amendment for the 3GPP SCM based on the key idea of unequal intra-cluster ray generation. More concretely, we apply a stochastic generation of the number of clusters via Poisson distribution; thereafter, we also apply a stochastic generation of target intra-cluster delay and angular spreads via exponential distributions. Based on these targets, a delay time and angle of arrival of intra-cluster rays are generated. Simulation results demonstrate an improved accuracy of the proposed amendment in terms of the distributions of the number of rays, intra-cluster delay spreads, and intra-cluster angular spreads.

The salient contributions are summarized as follows:

- This is the first study that holistically derives statistical propagation characteristics in the unexplored 95 GHz band based on a field measurement with the 4 GHz bandwidth (Sections II and III). We compare them with the 60 GHz [13] characteristics separately obtained in a similar scenario and highlight that the frequency difference in these two bands does not largely affect the trend of the LSPs, which are rather affected by environments. Hence, the usage of shared statistical parameters among 60–95 GHz is feasible given the same target scenarios.
- This study highlights that the equal characterization of the intra-cluster rays in the current 3GPP SCM does not necessarily lead to an accurate generation of the intra-cluster rays (Section IV-A). This fact is validated from the aforementioned measurement with 4 GHz bandwidth, where a large distinction between the measured distribution of the number of clusters, intra-cluster delay, and angular spreads are found.
- To solve this issue, this study proposes an amendment of unequal generation of intra-cluster rays, thereby providing an accurate CIR generation flow in a compatible manner with the 3GPP SCM (Section IV-B). The key idea behind the amendment is a stochastic generation of the intra-cluster parameters, such as the number of clusters and target delay/angular spreads. The proposed procedures are verified by the statistical consistency of the generated channel responses with the measured channel characteristics (Section V).

It should be noted that there are several comparative studies between 28GHz/60 GHz and the upper sub-THz band (e.g., 28 GHz vs. 140 GHz [25] and 60 GHz vs. 300 GHz [26]). Moreover, the channel models of the sub-THz band upper than 100 GHz have been recently proposed extensively in [27, 28]. However, the scope of this study is to investigate the generalizability of the current 3GPP SCM for the band around 100 GHz, i.e., the lower edge of the sub-THz band, and to provide a minimum but necessary amendment for the 3GPP SCM for this band. We believe that addressing this issue has been a longstanding void of the previous studies and is providing sufficient insight for the sub-THz band channel modeling. Hence, investigating the upper sub-THz band and comparing the proposed amendments with the other channel models for the upper sub-THz band are beyond the scope of this study.

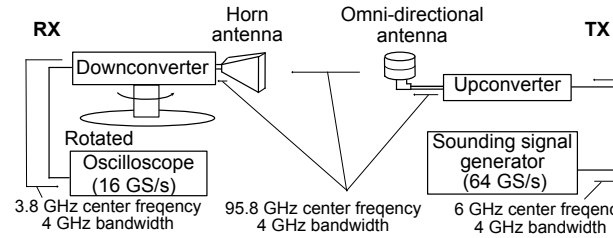

FIGURE 1. Channel sounding system for 95 GHz measurements.

The remainder of this article is as follows: Section II presents the 95 GHz multipath channel measurement in an indoor conference room environment. Section III analyzes the statistical parameters of the measured 95 GHz channel characteristics and compares them with the 60 GHz parameters. Section IV details the problem statement of the 3GPP SCM for a large-bandwidth use case based on the measurement results and proposes an amendment for unequal small-scale intra-cluster ray generation. Section V provides a numerical evaluation to validate the proposed amendment. Finally, Section VI provides a concluding remark.

II. MEASUREMENT SETUP OF 95 GHZ BAND IN CONFERENCE ROOM SCENARIO

A. CHANNEL SOUNDER SETUP

We developed a channel sounder capable of measuring a power delay profile (PDP) with a measurement bandwidth of 4 GHz at a center frequency of 95.8 GHz. The overall architecture is illustrated in Fig. 1. On the TX side, a 64 giga-sample/s arbitrary waveform generator is employed as a sounding signal generator. At this signal generator, modulated sounding signals with a bandwidth of 4 GHz at the carrier frequency of 6 GHz are generated and passed to an upconverter. The upconverter converts the carrier frequency of the sounding signal to 95.8 GHz, and the sounding signal is transmitted by the omnidirectional antenna in the TX. On the RX side, a rotatable horn antenna directionally receives the sounding signal. Subsequently, the downconverter converts the carrier frequency of the sounding signal to 3 GHz, and the sounding signal is fed into an oscilloscope with a sampling rate of 16 giga-samples/s. Finally, the oscilloscope calculates a PDP that represents multipath characteristics captured by the horn antenna. To generate the sounding signal and calculate the PDP, we employed the Keysight channel sounding software [29], which is one of the correlation-based channel sounding techniques. The measurement parameters are presented in Table I. Moreover, we conducted the validation of the channel sounding system in

TABLE 1. MEASUREMENT SETUP

RF frequency	95.8 GHz
Carrier frequency of sounding signal before TX upconversion (i.e., IF for TX)	6 GHz
Carrier frequency of sounding signal after RX downconversion (i.e., IF for RX)	3.8 GHz
Measurement bandwidth	4 GHz
Transmit power	9.3 dBm
Receiver antenna gain	25 dBi
Half-power beamwidth of receiver horn antenna	10°
Transmitter antenna gain	Omnidirectional in azimuth 4 dBi in elevation
Sampling frequency	16 GHz

an anechoic room, showing that the channel sounding system is capable of resolving multipath that arrives in the time difference of at least 1 ns and the angular difference of 20° [1]. For more detailed information, readers are encouraged to refer to [1].

B. MEASUREMENT SCENARIO

As shown in Fig. 2(a), we conducted a channel measurement in a small conference room as a typical use case of short-range communication in a high-frequency band. The conference room was approximately rectangular, and the floor plan is shown in Fig. 2(b). In the middle of the meeting room, desks were aligned in a rectangular shape. On one of the desks, the TX was located at a height of 0.15 m from the top of the desk. The RX was located at the same height as the TX along with the outer edge of the desks as shown in Fig. 2(b). We conducted the measurement at 8 RX locations, where the TX-RX distances were 1.00, 1.53, 2.00, 2.63, 3.00, 3.40, 3.64, and 4.00 m. This scenario was selected because it was one of the real use case scenarios considered in the earliest standardization activities of commercial mmWave communication systems, that is, the IEEE 802.15.3c and IEEE 802.11ad. To draw insight into the potential commercialization of 95 GHz communication systems in indoor short-range scenarios, we first examined the aforementioned measurement environment.

C. MEASUREMENT PROCEDURE

For each RX location, we conducted the channel measurement via the following procedure. First, we fixed the RX horn antenna so that the antenna boresight was aligned toward the direction of the TX omnidirectional antenna. This process was done by roughly aligning the horn antenna through a visual inspection and subsequently by rotating the horn antenna with a step of 1° while searching for the maximum power peak. When the maximum power peak was found, we set the RX horn antenna rotation angle as a reference angle of 0°. Hereinafter, a negative value of the angle denotes a counterclockwise rotation from the reference angle. Subsequently, we rotated the RX horn antenna −180° and

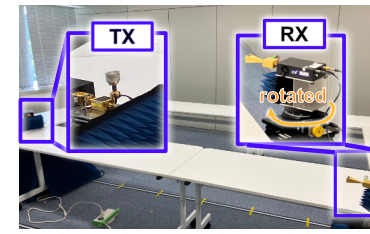

(a) Picture of the meeting room and RX setup at RX5.

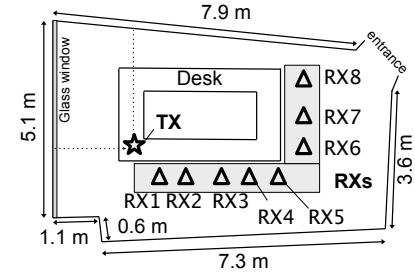

(b) Floor plan of the meeting room.

FIGURE 2. Floor plan and photograph of the measurement environment. The measurement was conducted at eight RX locations named RX1–RX8 with the TX-RX distances of 1.00, 1.53, 2.00, 2.63, 3.00, 3.40, 3.64, and 4.00 m, respectively.

started recording a PDP. From this starting angle, we rotated the horn antenna clockwise 175° with a step of 5°, and for each rotation angle, we recorded a PDP. Hence, the total number of resultant PDPs was 72 at each RX location.

The set of the recorded 72 PDPs referred to as the "raw power angular delay profile (PADP)" has the following two characteristics. First, the PDP for each RX antenna rotation angle exhibits 4098 power samples with a time resolution of 0.164 ns. Second, the maximum power peak observed in the PDP for each RX antenna rotation angle is located at 0 ns. This is because the RX and TX were not synchronized to obtain the absolute time of flight; hence, the only delay time relative to the strongest power peak is observed. Mathematically, the raw PADP is expressed as follows:

$$P_{\text{raw}}\left(\tau^{(\theta_{\text{RX}})},\, \theta_{\text{RX}}\right) \tag{1}$$

where $\theta_{\text{RX}} \in \{-180° + 5° \times n \mid n = 0,1, \ldots 71\}$ denotes the RX antenna rotation angle. The term $\tau^{(\theta_{\text{RX}})} \in \{n \times 0.164 \text{ ns} \mid n = -2048, -2047, \ldots, 2046, 2047\}$ denotes the delay time relative to the maximum power peak. Note that the absolute time of the maximum power peak is different for each θ_{RX}; accordingly, $\tau^{(\theta_{\text{RX}})}$ is specific to θ_{RX}.

For channel modeling, the raw PADP should be aligned so that for all θ_{RX}, the delay time is the absolute time flight. The resultant PADP is termed the "time-aligned PADP" and is mathematically expressed as

$$P_{\text{align}}(\tau, \theta_{\text{RX}}) = P_{\text{raw}}\left(\tau - T_{\text{diff,LoS}}^{(\theta_{\text{RX}})},\, \theta_{\text{RX}}\right) \tag{2}$$

where $T_{\text{diff,LoS}}^{(\theta_{\text{RX}})}$ represents the time of flight of the maximum power peak at the antenna rotation angle θ_{RX} relative to the LoS ray arrival time. However, this measurement was

TABLE 2. STATISTICAL PARAMETERS FOR CONFERENCE ROOM SHORT-RANGE COMMUNICATION SCENARIO AT 95 GHZ

Extracted Parameters		**Our 95 GHz measurement in conference room**	Our 60 GHz measurement in conference room[*5]	3GPP SCM for indoor office in LoS at 95 GHz
Delay Spread DS[*1] $lgDS = \log_{10}(DS/1\text{s})$	μ_{lgDS}[*3]	**−8.30**	−8.60	−7.71
	σ_{lgDS}[*4]	**0.13**	0.34	0.18
AoA Spread ASA[*2] $lgASA = \log_{10}(ASA/1°)$	μ_{lgASA}	**1.34**	1.33	1.40
	σ_{lgASA}	**0.19**	0.28	0.35
K-Factor K [dB]	μ_{K}	**7.30**	11.8	7
	σ_{K}	**5.93**	6.18	4
Cross-correlations	ASA vs. DS	**0.83**	0.88	0.8
	DS vs. K	**−0.78**	−0.94	−0.5
	ASA vs. K	**−0.99**	−0.95	0
Delay scaling factor r_τ		**1.54**	1.29	3.6
Number of clusters N		**10**	10	15
Per-cluster shadow fading standard deviation (ζ) in [dB]		**5.37**	4.84	6
Path loss exponent		**1.74**	1.69	1.73
Shadow fading standard deviation (σ) [dB]		**0.83**	0.74	3

NOTE 1: DS denotes the root mean square (RMS) delay spread. NOTE 2: ASA denotes the RMS azimuth spread of arrival angles.
NOTE 3: μ_{lgX} denotes the mean of the logarithmized parameter X.
NOTE 4: σ_{lgX} denotes the standard deviation of the logarithmized parameter X.
NOTE 5: A cut-off level of –25 dB relative to the LoS ray for the MPC analysis is applied to ensure the compatibility to the 3GPP SCM [5] whereas [13] applied –40 dB threshold. Hence, the parameter values are different from the table in [13].

conducted without any knowledge of $T_{\text{diff,LoS}}^{(\theta_{\text{RX}})}$ as discussed above, and, we should estimate $T_{\text{diff,LoS}}^{(\theta_{\text{RX}})}$ from $P_{\text{raw}}\left(\tau^{(\theta_{\text{RX}})}, \theta_{\text{RX}}\right)$. To this end, we leveraged the recently proposed time-alignment algorithm, which was well-validated in the same conference room scenario [30]. In this paper, we do not detail this time alignment algorithm to focus on the 95 GHz channel measurement. Readers are encouraged to consult [30] for more detail and [1] for a more concrete motivating example.

III. STATISTICAL LARGE-SCALE PARAMETER CHARACTERIZATIONS OF 95 GHZ SHORT-RANGE COMMUNICATION SCENARIO IN CONCERENCE ROOM

Table II shows the statistical characteristics found in the 95 GHz and 60 GHz measurements in a similar conference room [13]. Moreover, Table II shows the same parameters in the 3GPP SCM report for indoor offices at 95 GHz. These parameters are calculated with the multipath components (MPCs) found by applying the successive interference cancellation algorithm [31] with the power threshold of −25 dB relative to the LoS power peak. The value of −25 dB is intended to be compatible with the 3GPP SCM where the clusters with the power of −25 dB are cut off [5]. By using these MPCs, delay spread and azimuth AoA spread are calculated. Subsequently, the MPCs are clustered by the K-power means algorithm [31], and based on the clustering results, the K-factor, delay scaling factor, and per-cluster shadow fading term are calculated.

A. DISTRIBUTIONS OF DELAY SPREAD, ANGULAR SPREAD, AND K-FACTOR

Figs. 3–5 shows the distribution of the delay spread, azimuth AoA spread, and K-factor found from the

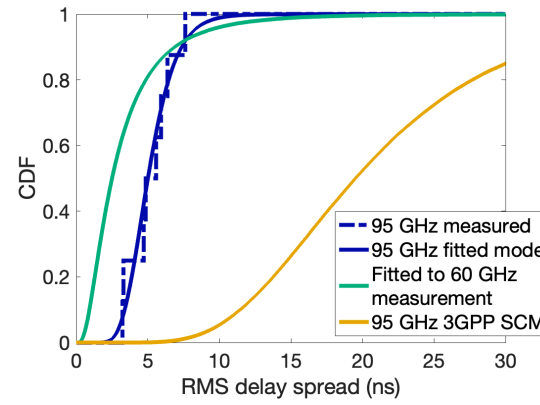

FIGURE 3. Delay spread distributions.

measurement and the distribution models for 60 GHz in a similar conference room environment [13] and 3GPP SCM for 95 GHz in indoor office scenarios [5]. The distribution models for the delay spread and azimuth AoA spread depicted in smooth lines are the log-normal distribution with a base of 10, and the mean and standard deviation are summarized in Table II.

This comparison dictates that the distributions of the delay spread and azimuth AoA spread found at the 95 GHz band are more similar to the model at 60 GHz in a similar environment than to the 3GPP SCM at 95 GHz for indoor office scenarios. More concretely, as shown in Fig. 3, the delay spread in the 3GPP SCM tends to be larger than the distributions found in conference rooms. This can be attributed to the room size where the 3GPP SCM considers a larger office room than the conference room, and the delayed wave can reach in a longer delay time in the former office room. Moreover, as shown in Fig. 4, the azimuth AoA spread in the 3GPP SCM distributes in larger values

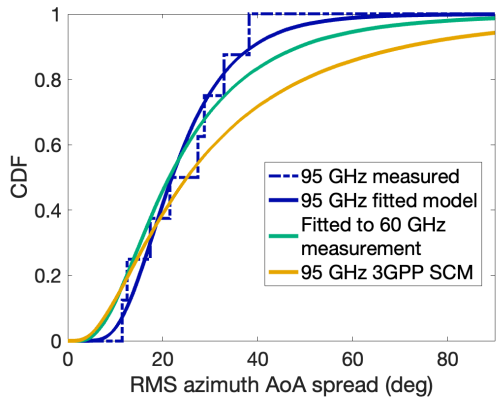

FIGURE 4. **Azimuth AoA spread distributions.**

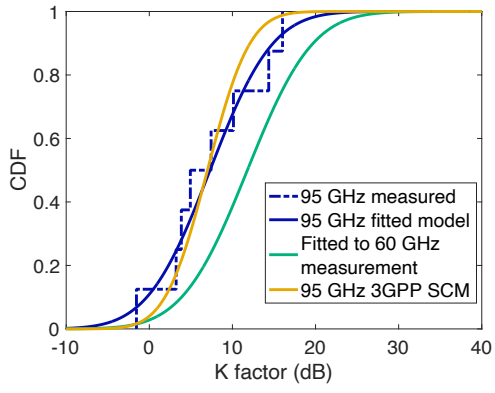

FIGURE 5. **K factor distributions.**

than in the other results obtained in the conference room scenarios. The rationale behind this observation is as follows: The 3GPP SCM considers a longer distance communication, and the multipath waves can possess a comparable power with the LoS path. Contrarily, the conference room scenario exhibits a shorter communication range, where the power of the LoS ray is basically larger than the other multipaths. Hence, the former scenario considered by the 3GPP SCM can result in a more angular power dispersion, leading to a larger AoA spread.

It should be noted that the K-factor distribution is different between the results at 95 GHz and 60 GHz in Fig. 5, where the K-factor at 60 GHz distributes in a larger value. However, this may not be attributed to the frequency difference, but be attributed to the difference in the RX positions in these two measurements. In this measurement at 95 GHz, the RX was placed on two sides of the desk as shown in Fig. 2 while in the measurement at 60 GHz, the RX was also placed on the opposite sides of the desk at the TX-RX distance of 1m, 2m, 3m. Moreover, in the 60 GHz measurement, the RX was not placed in the TX-RX distance of 1.53m, 2.63 m, 3.40 m, and 3.64 m. Hence, in the 60 GHz measurement, the LoS ray tends to be dominant, leading to the larger K-factor. Hence, we conclude that rather than the frequency difference, a measurement environment and scenario are a dominant factor to affect these statistical parameters.

B. CORRELATIONS AMONG DELAY SPREAD, ANGULAR SPREAD, AND K-FACTOR

From Table II, the cross-correlations among the delay spread, azimuth AoA spread, and K-factor exhibit a similar trend among the 95 GHz measurement, fitted model to the 60 GHz measurement, and 3GPP SCM, except for the correlation between the azimuth AoA spread and K-factor. More concretely, the 3GPP SCM set this correlation as zero whereas the other results found in the conference room exhibit a strong negative correlation.

This strong negative cross-correlation in the conference room scenario can be explained by the confounding effect w.r.t. the RX-TX distance; With an increase in the RX-TX distance, the reflective multipaths become dominant relative to the LoS ray. This affects both the K-factor and the azimuth AoA spread, where the K-factor decreases and the azimuth AoA spread increases simultaneously. This characteristic is more apparent in the short-range conference room scenario where the level of the LoS dominance is sensitive to the TX-RX distance. For instance, at the TX-RX distance of 1m, the LoS ray is dominant (i.e., K factor was 14 dB) while at the distance of 4 m the LoS ray is much less dominant (K factor was -1.54 dB). Thus, this difference in the cross-correlation between K-factor and azimuth AoA spread is attributed to the communication scenario.

C. DELAY SCALING PARAMETER

In the 3GPP SCM [5], the cluster excess delay time τ_c is assumed to follow an exponential distribution:

$$C_\tau \tau_c / DS \sim \mathrm{Exp}(1/r), \tag{3}$$

where $\mathrm{Exp}(\cdot)$ represents the exponential distribution with the argument of the rate parameter, DS represents the delay spread of the target RX location for modeling the cluster delay time. r is the delay scaling parameter and dictates the dispersion level of the cluster excess delay This section analyzes this delay scaling parameters for the aforementioned scenarios. Note that C_τ is the additional scaling factor that is detailed in [5].

Fig. 6 shows the distribution of the normalized cluster excess delay time found in the 95 GHz measurement with those of the 60 GHz in the similar scenario and 3GPP SCM. Normalized cluster excess delay is referred to as the left-hand-side in (3) and hence is dimensionless. From Fig. 6, we can see that the distributions found in the 95 GHz measurement come close to the fitted model and the 60 GHz model while the 3GPP SCM deviates from them. This difference can be attributed to the scenario. In the former short-range communication scenario in the conference room, the cluster delay time tends to be smaller because the reflective materials, such as walls and windows, are relatively close to the TX and RX. Contrary, in the longer-range communication scenario in a larger office room considered by the 3GPP SCM, these reflective materials are

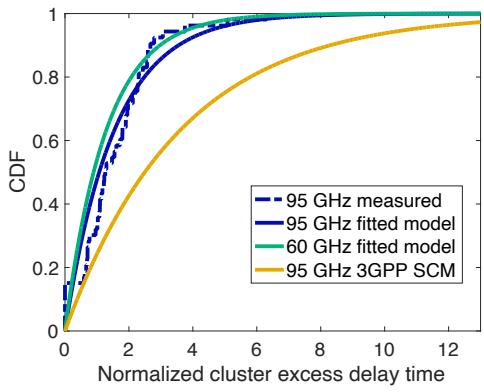

FIGURE 6. **Normalized cluster excess delay distributions.**

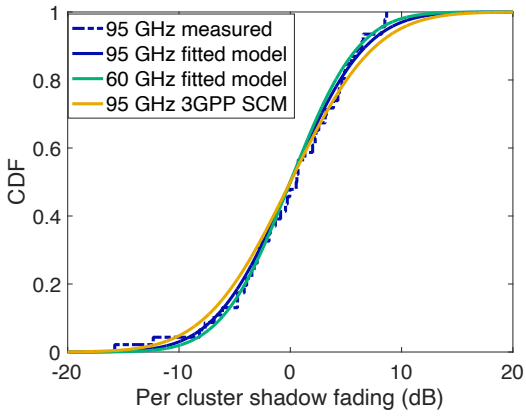

FIGURE 7. **Per-cluster shadow fading distributions.**

further from the TX and RX, resulting in larger values of cluster excess delay time.

D. PER-CLUSTER SHADOW FADING TERM

In the 3GPP SCM, the cluster powers, i.e., the total power of the MPCs in each NLoS cluster, follow the exponential decay model:

$$\Omega \exp\left(-\tau_{\text{norm}} \cdot \frac{r-1}{r}\right) \cdot 10^{-\frac{Z}{10}} \tag{4}$$

where $\tau_{\text{norm}} := C_\tau \tau_c / DS$ and Ω is the constant term in Watts. $Z \sim \mathcal{N}(0, \zeta^2)$ represents the power dispersion term from the exponential decay, which is referred to as the per-cluster shadow fading term. The larger standard deviation of the per-cluster shadow fading indicates that the mechanism of multipath arrivals cannot be explained only with the free-space path loss models (ex, due to scattering effects or blockage effects); hence, this term dictates the complexity of the multipath arrival mechanism.

Fig. 7 shows the distribution of the per-cluster shadow fading. From Fig. 7, we can see that the measurement results and the three distribution models do not exhibit significant differences in the dispersion of the per-cluster shadow fading. Hence, this term is not only invariant concerning the frequency bands as seen from the comparison with the 60 GHz model in the conference room scenario but also invariant concerning the scenarios as seen from the comparison with 95 GHz 3GPP SCM.

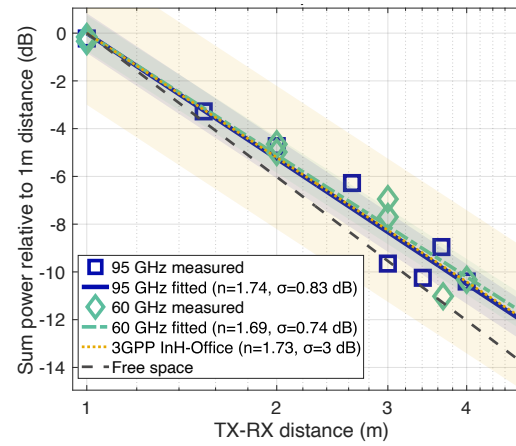

FIGURE 8. **Sum power decay with respect to TX-RX distance and path loss models (Shaded area represents the standard deviation area in each corresponding line).**

E. OMNIDIRECTIONAL PATH-LOSS MODEL

Finally, we derived a path loss model based on a well-accepted close-in free-space reference distance path loss model [32]. In the model, the path loss $\text{PL}(d, f)$ (dB) at the distance d and frequency f is formulated as follows:

$$\text{PL}(d, f) = \text{FSPL}(d_0, f) + 10n \log_{10}(d/d_0) + \chi_\sigma, \tag{5}$$

where $\text{FSPL}(d_0, f)$ (dB) denotes the free space path loss at the reference distance d_0 in the same frequency. The terms n and $\chi_\sigma \sim \mathcal{N}(0, \sigma^2)$, denote the path loss exponent and the shadow fading term, respectively, where σ^2 is the standard deviation of the shadow fading term. These are found by the least squared fitting with the x-variable of distance and y-variable of the sum of received power in the omnidirectional PDP (i.e., the integral of the PADP with respect to the antenna rotation angle) above –30 dB of the maximum power peak. Noticeably, the 3GPP SCM also uses this model for indoor scenarios with $n = 1.7$ and $\sigma = 3$ dB as the LoS indoor hotspot (InH)-office model; hence, we compare the path loss model found by this measurement with the 3GPP SCM.

Fig. 8 shows the power degradation with respect to the TX-RX distance. In Fig. 8, the shaded area represents the points within the standard deviation from the power decay line. From Fig. 8, we can find that the path loss model found at 95 GHz and 60 GHz did not exhibit significant differences in both path loss exponent and shadow fading standard deviation. Hence, these two bands can be analyzed by integrated path loss models. Comparing the result at 95 GHz in the desktop scenario with the 3GPP SCM InH-office scenario, the latter model exhibits a larger standard deviation. This is attributed to the simplicity of the considered channel environment at the 95 GHz desktop

scenario; hence, the environment difference is the major factor that impacts the statistical characteristics of the path loss.

F. SUMMARY

As detailed in the above evaluations, the 95 GHz and 60 GHz bands exhibit similar statistical parameters in the conference room desktop environment while the scenario difference results in the distinction in the statistical parameters. Hence, in the band ranging from 60 GHz to 100 GHz, frequency difference is not as a major factor as the scenario difference. Recalling that these parameters are related to the model of the multipath clusters [5], these results indicate that given the same target environment, we can develop an integrated large-scale multipath channel model for the cluster generation for the 60 GHz–100 GHz bands.

Nonetheless, at the 90 GHz–100 GHz, the usage of a larger bandwidth than the 60 GHz band is expected; hence, an accurate model of small-scale sub-paths is required. In the next section, we highlight that the 3GPP SCM is not necessarily suited for the large-bandwidth use case, and we propose an improved channel generation procedure for the large-bandwidth use cases.

IV. IMPROVED SMALL-SCALE CHANNEL GENERATION PROCEDURE IN FOR CONFERENCE ROOM SHORT-RANGE COMMUNICATION

This section proposes a channel generation procedure to reproduce the channel characteristics for link-level simulations. The objective of this procedure is to generate a channel impulse response formalized as follows:

$$H(\tau,\phi)=\sum_{n=1}^{N}\sum_{m=1}^{M_n}\sqrt{P_{n,m}}\mathrm{e}^{j\Phi_{n,m}}\delta\left(t-\tau_{n,m}\right)\cdot\delta\left(\phi-\phi_{n,m}\right), \tag{6}$$

where

$$\Phi_{n,m}\sim\mathrm{uniform}(-180°,180°); \tag{7}$$

$$\sum_{N=1}^{N}\sum_{m=1}^{M_n}P_{n,m}=1; \tag{8}$$

In the above equations, n and m are the indices of the cluster and intra-cluster subpaths, respectively. $\Phi_{n,m}$ represents the phase of the corresponding subpath and is sampled in an i.i.d. manner. The terms $P_{n,m}$, $\tau_{n,m}$, and $\phi_{n,m}$ represent the power, excess delay, and the relative azimuth AoA of the m^{th} subpath in the n^{th} cluster. M_n represents the number of subpaths in the n^{th} cluster, and $\delta(\cdot)$ is the Dirac delta function. The sum of sub-path power is normalized so that the developers can use arbitrary path loss models, which is the general assumption for the 3GPP SCM.

The channel generation procedure generates $P_{n,m}$, $\tau_{n,m}$, and $\phi_{n,m}$, statistically because this suffices to compose the channel impulse response as in (6). Generally, this procedure is subdivided into the two steps: cluster-wise generation and intra-cluster-wise generation. More concretely, a general representation of $P_{n,m}$, $\tau_{n,m}$, and $\phi_{n,m}$ are divided into the cluster-wise term and its offset from the cluster-wise term as follows:

$$P_{n,m}=P_nP'_{n,m},\ \tau_{n,m}=\tau_n+\tau'_{n,m},\quad \phi_{n,m}=\phi_n+\phi'_{n,m}, \tag{9}$$

where the terms, P_n, τ_n, and ϕ_n represent the sum power, delay, and azimuth AoA of the nth cluster, and $P'_{n,m}$, $\tau'_{n,m}$, and $\phi'_{n,m}$ denote the offset values from the respective variables. This section mainly focuses on the generation procedure of the latter intra-cluster variables because the usage of large bandwidth and high directional antennas requires an accurate statistical modeling of the intra-cluster-wise variables.

Note that the delay and azimuth AoAs are relative to the LoS ray arrival time and its azimuth AoA, respectively. By following the 3GPP SCM, we consider the first cluster as the LoS cluster, implying that $\tau_1=0$ ns and $\phi_n=0°$.

A. PROBLEM IDENTIFICATION

1) REVIEW OF GENERATION PROCEDURE OF INTRA-CLUSTER VARIABLES IN 3GPP SCM

The 3GPP SCM defines the generation procedure of intra-cluster-wise variables for use cases with a large bandwidth. First, we revisit this procedure for problem identification.

In the 3GPP SCM, an equal number of intra-cluster subpaths are generated for all clusters; accordingly, an equal number of samples for the intra-cluster-wise offset variables are generated in each cluster. Let M denote the number of intra-cluster subpaths. First, for each cluster n, the delay offsets of intra-cluster subpaths $\tau'_{n,1},\ldots,\tau'_{n,M}$ is generated as follows:

$$\tau''_{n,1},\ldots\tau''_{n,M}\sim\mathrm{uniform}(0,2c_{DS}), \tag{10}$$

$$\tau'_{n,m}=\tau''_{n,m}-\min_m\left\{\tau''_{n,m}\right\},\ \text{for}\ m=1,\ldots M \tag{11}$$

where c_{DS} denotes the per-cluster delay spread given as an identical value of all clusters. Secondly, the azimuth AoA offsets of the intra-cluster subpaths $\phi'_{n,1},\ldots,\phi'_{n,M}$ are generated as follows:

$$\alpha_{n,1},\ldots\alpha_{n,M}\sim\mathrm{uniform}(-2,2), \tag{12}$$

$$\phi'_{n,m}=\alpha_{n,m}c_{ASA},\ \text{for}\ m=1,\ldots M \tag{13}$$

where c_{ASA} denotes the per-cluster azimuth AoA spread given as an identical value of all clusters. Finally, the intra-cluster power ratios $P'_{n,1},\ldots P'_{n,M}$ are calculated as follows:

$$P''_{n,m}=\exp\left(-\frac{\tau'_{n,m}}{c_{DS}}\right)\cdot\exp\left(-\frac{\sqrt{2}|\alpha_{n,m}|}{c_{ASA}}\right), \tag{14}$$

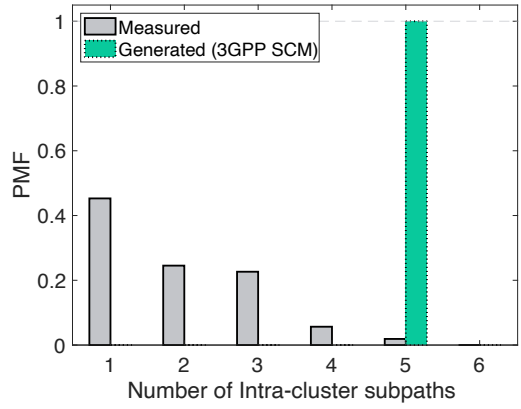

FIGURE 9. **Distribution of the number of intra-cluster subpaths.**

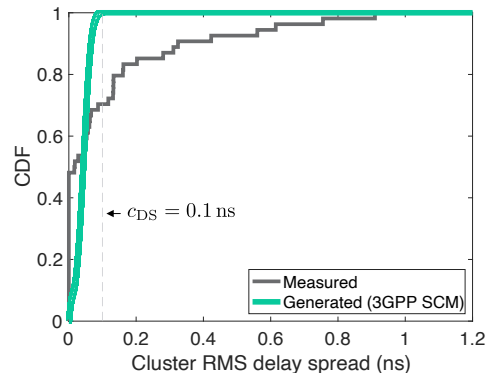

FIGURE 10. **Distribution of intra-cluster delay spread.**

$$P'_{n,m} = P''_{n,m} / \sum_{m=1}^{M} P''_{n,m}. \tag{15}$$

Thus, combining these values with the cluster-wise variables separately generated by the procedure defined in the 3GPP SCM, we can finally obtain one sample of channel responses $H(\tau, \phi)$ in (6).

2) PROBLEM IDENTIFICATION: EQUAL STATISTICAL CHARACTERISTICS FOR INTRA-CLUSTER VARIABLES

As indicated in (10)–(15), in the 3GPP SCM, intra-cluster-wise variables are generated subject to the same values of the number of clusters M, per-cluster delay spread c_{DS} and per-cluster azimuth AoA spread c_{ASA} for all clusters. This fact implies that the generated intra-cluster subpaths possess the same statistical characteristics.

However, this equal statistical characteristic of the intra-cluster subpaths for all clusters is far from reality. Figs. 9–11 show the distribution of the number of intra-cluster subpaths, per-cluster delay spread, and per-cluster azimuth AoA spread found from our measurement. Moreover, in the same figure, we plot the distributions of these variables yielded by the 3GPP SCM channel generation procedures (10)–(15). The parameters are set as: $M = 5$, $c_{DS} = 0.1$ ns, and $c_{ASA} = 0.85°$, which are the maximum, average, and average values, respectively, found from our measurement. Note that these figures are the partial results, which will be shown in Section V later again. From Fig. 9, we can find that the number of intra-cluster subpaths M is different from cluster to cluster, and that we cannot represent it with one value. Moreover, from Figs. 10 and 11, the measured per-cluster delay and azimuth AoA spreads distribute to be zero intensively and partially spread for larger values; namely, the distribution possesses multi-modality. The reason is in the difference between the clusters with only one subpath and those with more than one subpath. When the cluster possesses only one subpath, the per-cluster delay and azimuth AoA spread are deterministically zero; otherwise, these values distribute for more than the zero value. These characteristics cannot be captured by the current 3GPP SCM treating the cluster equally with the uniform values of c_{DS} and c_{ASA}. This problem is cast as the "equal characterization problem of intra-cluster variables," which are summarized as follows:

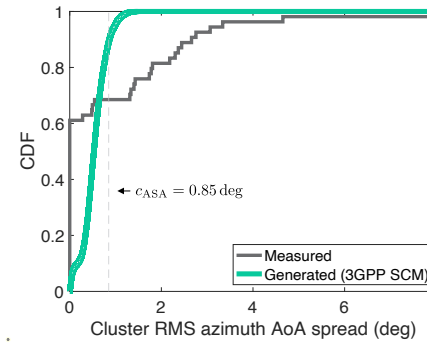

FIGURE 11. **Distribution of intra-cluster azimuth AoA spread.**

Remark 1 (Equal characterization problem of intra-cluster variables in 3GPP SCM). In the channel generation procedure of the 3GPP SCM, the intra-cluster variables are generated subject to the equal parameter values of the number of clusters M, c_{DS}, and c_{ASA} for all clusters. This procedure hardly generates real channel characteristics, which can be different from cluster to cluster.

B. PROPOSED CHANNEL GENERATION PROCEDURE

1) AMENDMENT: GENERATING UNEQUAL SUBPATH CHARACTERISTICS

To solve the problem, we amend the 3GPP SCM channel generation procedure. More concretely, to differentiate the intra-cluster-wise characteristics among clusters, we apply the statistical generation of the number of intra-cluster subpaths M, cluster delay spread c_{DS}, and cluster azimuth AoA spread c_{ASA}. First, we model the number of intra-cluster subpaths M as the following Poisson distribution:

$$\mathbb{P}(M = m) = \frac{\lambda_M^{m-1} \mathrm{e}^{-\lambda_M}}{(m-1)!}, \qquad (m = 1, 2, \ldots), \tag{16}$$

where λ_M is the parameter of the Poisson distribution and should be estimated with the maximum likelihood method. Based on this model, for each cluster n, the number of subpaths M_n are generated as follows:

$$M_n - 1 \sim \mathrm{Poi}(\lambda_M^\star), \tag{17}$$

where $\mathrm{Poi}(\cdot)$ denotes the Poisson distribution with the argument rate parameter, and $\lambda_M^\star = 0.94$ is the maximum likely parameter found from the measurement. Clearly, M_n is subject to the subscript of the cluster index n; hence, the number of intra-cluster subpaths is unequal from cluster to cluster.

Likewise, the per-cluster spread values c_{DS} and c_{ASA} are also generated from the statistical model for each cluster, not reusing an equal value. Recalling that these values are deterministically zero if $M_n = 1$, we develop a statistical model mainly for the clusters with more than one subpaths. For such clusters, the per-cluster spread values c_{DS} and c_{ASA} are both modeled as exponential distributions, which is given as follows:

$$p(c_s | M_n > 1) = \lambda_{c_s} \mathrm{e}^{-\lambda_{c_s} c_s}, \tag{18}$$

where $p(\cdot\,|\,\cdot)$ is the conditional probability distribution function, the subscript $s \in \{DS, ASA\}$ denotes the delay or azimuth AoA spread, and λ_{c_s} is the rate parameter, which is estimated to fit the measurement data with a maximum likelihood estimation method. Note that for $M_n = 1$, $p(c_s | M_n = 1) = \delta(c_s)$, where $\delta(\cdot)$ is the Diac's delta function. Based on these models, for each cluster n, we generate the per-cluster delay spread $c_{DS,n}$ and per-cluster azimuth AoA spread $c_{ASA,n}$ as follows:

$$\begin{aligned} c_{s,n} &= 0, \quad \text{if} \quad M_n = 1, \\ c_{s,n} &\sim \mathrm{Exp}(\lambda_{c_s}^\star), \quad \text{otherwise.} \end{aligned} \tag{19}$$

where $\mathrm{Exp}(\cdot)$ denotes the Poisson distribution with the argument rate parameter, and $\lambda_{c_s}^\star$ is the maximum likely parameter for $s \in \{DS, ASA\}$ where $\lambda_{c_{DS}}^\star = 4.88$ and $\lambda_{c_{ASA}}^\star = 0.62$. Clearly, $c_{DS,n}$ and $c_{ASA,n}$ is subject to the cluster index n; hence, these variables are also different from cluster to cluster.

After the generation of these variables, we generate $\tau'_{n,1}, \ldots, \tau'_{n,M}$, $\phi'_{n,1}, \ldots, \phi'_{n,M}$, and $P'_{n,1}, \ldots P'_{n,M}$ with the same procedure as (10)–(15). However, as for the delay offset values $\tau'_{n,1}, \ldots, \tau'_{n,M}$, we modify the coefficient in the upper limit of the uniform distribution as follows:

$$\tau''_{n,1}, \ldots \tau''_{n,M} \sim \mathrm{uniform}(0, 10 c_{DS}), \tag{20}$$

which is heuristically found to fit the measurement results.

2) SUMMARY: COMPLETE ALGORITHM OF PROPOSED CHANNEL GENERATION PROCEDURE

Fig. 12 shows the complete algorithm of the proposed channel generation procedure including both the intra-cluster-wise a cluster-wise parameter generation method. As for the cluster-wise parameter generation, we mostly follow the 3GPP SCM. Therein, we generate a target a delay spread value, azimuth AoA spread value, and K-factor value from a multivariate Gaussian distribution

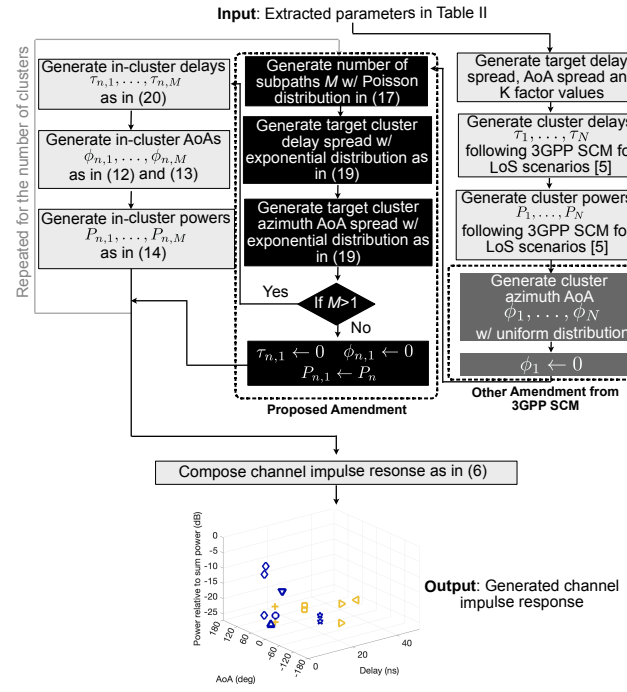

FIGURE 12. Overview of proposed channel generation procedure.

where the parameter table is input from Table II. Subsequently, the cluster excess delay values $\tau_1, \ldots, \tau_N$ and cluster power values $P_1, \ldots, P_N$ are generated by following the 3GPP SCM, where the cluster excess delay values are sampled from an exponential distribution in (3), and the cluster power values are calculated from the exponential decay function in (4) [5]. For the cluster azimuth AoA values $\phi_1, \ldots, \phi_N$, exceptionally, we sample them from a uniform distribution [13]:

$$\phi_1 = 0, \phi_2 \ldots, \phi_N \sim \mathrm{uniform}(-130°, 130°), \tag{21}$$

where the upper and lower limits of the uniform distribution are found to fit the measured azimuth AoA distribution. This procedure is opposed to the original 3GPP SCM that applied a wrapped Gaussian distribution, which are found to mismatch the measured azimuth AoA distributions in the conference room short-range communication scenario in [13]. Note that the azimuth AoA of the first cluster is forced to be zero because the first cluster includes the LoS ray, which gives us a standard azimuth AoA.

Subsequently, the intra-cluster parameters are generated by including the proposed amendment. Finally, the channel impulse response is composed of the generated variables as in (6).

V. NUMERICAL EVALUATIONS

A. EVALUATION METHODOLOGIES

We evaluate the proposed channel generation procedure by providing the characteristics of the generated channel impulse response and the corresponding characteristics

obtained via the measurement. To validate the proposed methodologies, we perform the comparisons with the baseline without the proposed amendment detailed in Section IV-B. Moreover, this baseline does not apply the uniform distribution-based cluster azimuth AoA generation procedure in (21); instead, the baseline applies the wrapped Gaussian distribution in the current 3GPP SCM [5]. Hence, the baseline is cast as the application of the current 3GPP SCM to the conference room scenario at the 95 GHz band. Note that to ensure a fair comparison, this baseline also uses the parameter table in Table II for the 95 GHz conference room scenario, and we focus only on the effectiveness of the proposed amendment.

In this baseline, we do not use the proposed amendment, which implies that we assign the constant values for the intra-cluster subpaths M, cluster delay spread c_{DS}, and cluster azimuth AoA spread c_{ASA} as in the 3GPP SCM. We set these values as follows: $M = 5$, $c_{DS} = 0.1$ ns, and $c_{ASA} = 0.85°$, where the number of the intra-cluster subpaths is set as the maximum number observed in the measurement, and the spread values are set as the average values observed in the measurement.

The evaluation methodology is as follows: First, we sample 1000 channel responses from the proposed and baseline algorithm. Subsequently, from each channel response sample, we re-calculate the variables of interest, such as delay spread, azimuth AoA spread, K-factor, and per-cluster spread values, and draw an empirical distribution of these variables for 1000 samples. This empirical distribution is compared with that found from the measurement detailed in Section II.

B. OUTLOOK OF GENERATED CHANNEL IMPULSE RESPONSE

First, we analyze the characteristics of the generated channel impulse responses with regard to delay and power. Fig. 13 shows the excess delay and power of each MPC found by the measurement, which are regarded as ground-truth values, and the other figures show an example generated in the proposed generation framework. The generated channel impulse responses with both baseline and proposed procedure well capture the characteristics of the ground-truth channel impulse response in the domain of excess delay and power. However, comparing Figs. 13(b) and 13(c), we can find that the proposed channel generation framework leads to a non-uniform number of intra-cluster subpaths, whereas baseline 2 generates a uniform number of intra-cluster subpaths, that is, $M = 5$ subpaths for all the clusters. This is due to the proposed amendment in (17) where the number of generated intra-cluster subpaths is statistically determined by a Poisson distribution.

Fig. 14 presents the characteristics of the same MPCs but in terms of excess delay and azimuth AoA. As shown in Fig. 14(a), the impulses found in the measurement are dispersed in a wide range of angles, while the generated impulses with the baseline in Fig. 14(b) do not exhibit this characteristic, where the AoAs of the generated MPCs are concentrated on approximately 80° and 270°. This is due to

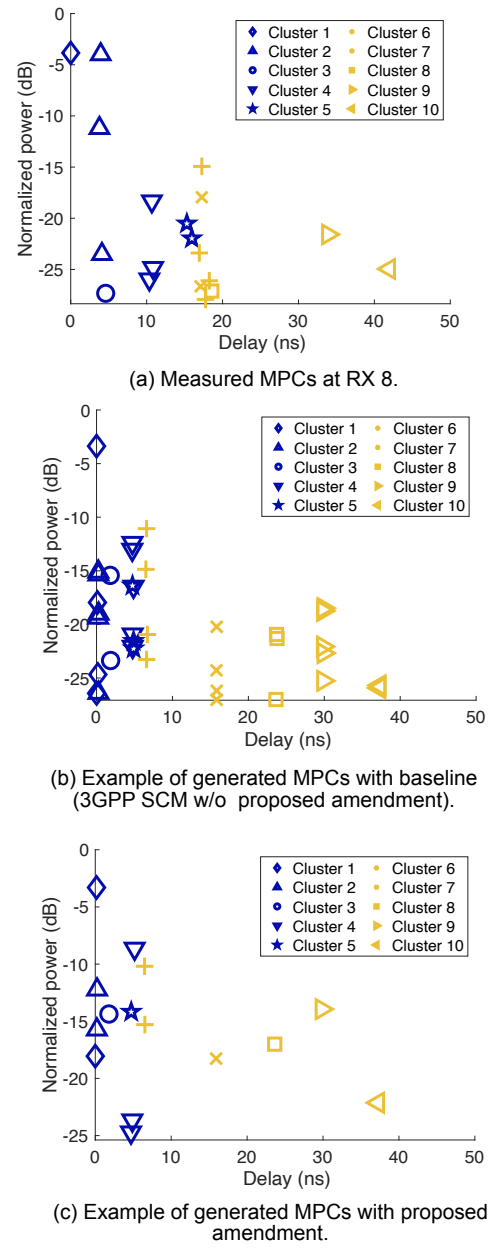

(a) Measured MPCs at RX 8.

(b) Example of generated MPCs with baseline (3GPP SCM w/o proposed amendment).

(c) Example of generated MPCs with proposed amendment.

FIGURE 13. Delay vs. power of measured and generated MPCs.

the inaccuracy of the wrapped Gaussian assumption identified in [13]. Meanwhile, the AoAs generated by the proposed procedure in Fig. 14(c) are dispersed in the angle domain, exhibiting a more similar characteristic to the measurement.

C. IMPROVEMENTS FROM PROPOSED UNEQUAL SUBPATH GENRERATION PROCEDURE

Second, we evaluate the benefit of the proposed unequal generation of subpath characteristics for each cluster. Fig. 15 shows the distribution of the number of intra-cluster subpaths measured and generated from the baseline and proposed channel generation procedure. The baseline generates the same number of intra-cluster subpaths in all the clusters, resulting in a deterministic number of intra-

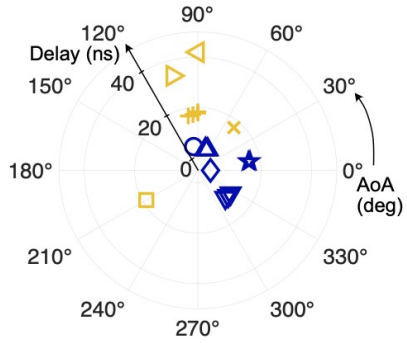

(a) Measured MPCs at RX 8.

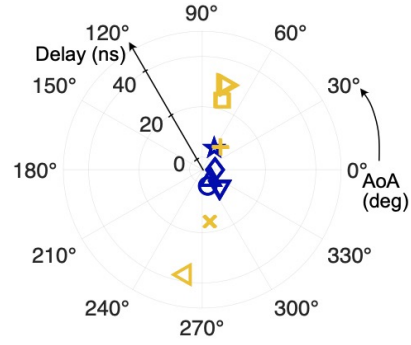

(b) Example of generated MPCs with baseline (3GPP SCM w/o proposed amendment).

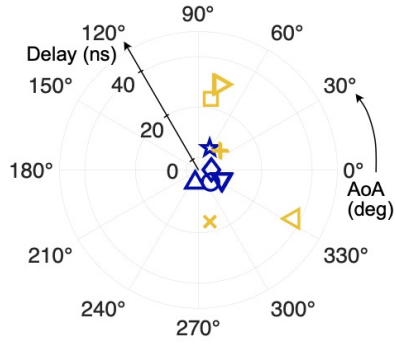

(c) Example of generated MPCs with proposed amendment.

FIGURE 14. Delay vs. power of measured and generated MPCs.

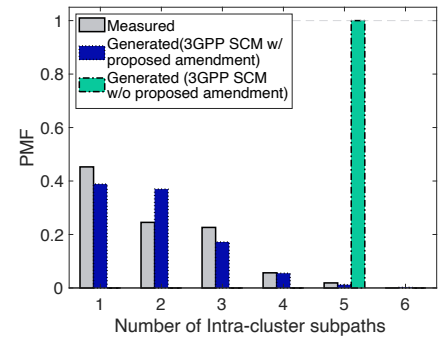

FIGURE 15. Distribution of the number of intra-cluster subpaths.

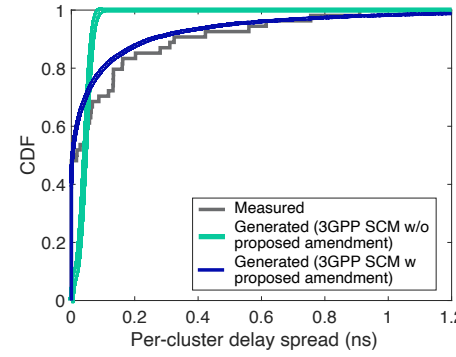

FIGURE 16. Distribution of per-cluster delay spread.

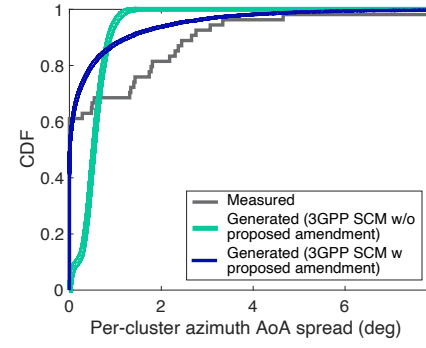

FIGURE 17. Distribution of per-cluster azimuth AoA spread.

cluster subpaths. Meanwhile, the proposed procedure randomly generates the intra-cluster subpaths according to the Poisson distribution with the maximum-likely parameter $\lambda_M^\star$, thereby reaching a more accurate distribution of the number of intra-cluster subpaths.

Figs. 16 and 17 show the distributions of the per-cluster delay spread and azimuth AoA spread, respectively, found in the measurement and in the generated channel responses with the baseline and the proposed procedure. For the per-cluster delay spread shown in Fig. 16, the proposed procedure generates a broader range of samples than the baseline, which is closer to the measured per-cluster delay spread distribution. This is due to the generation mechanism of the per-cluster delay spread values expressed by (19) as opposed to the baseline which gives only one value as a per-cluster delay spread. The same improvement can be found in the per-cluster azimuth AoA spread, as shown in Fig. 17. Regardless of the distinction between the measurement and generation with the proposed method, the trend of the azimuth AoA spread generated with the proposed method is rather close to the measurement than the 3GPP SCM without proposed amendment.

D. VALIDATION FOR LARGE-SCALE PARAMETERS OF GENERATED CHANNEL RESPONSES

Finally, we evaluate the delay spread, azimuth AoA spread, and K-factor calculated using the generated channel responses, thereby verifying that the proposed procedure yields channel responses consistent with the measurement

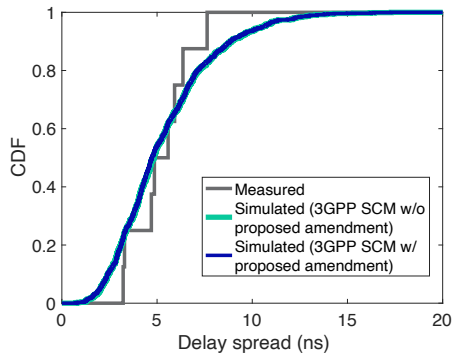

FIGURE 18. **Delay spread distribution.**

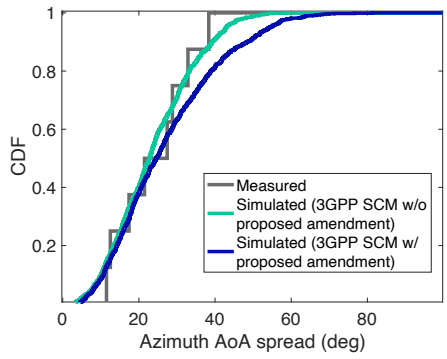

FIGURE 19. **Azimuth AoA spread distribution.**

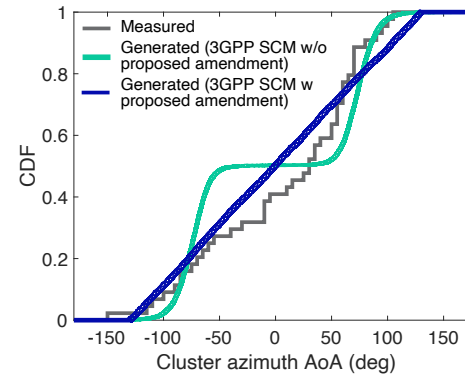

FIGURE 20. **Cluster azimuth AoA distribution.**

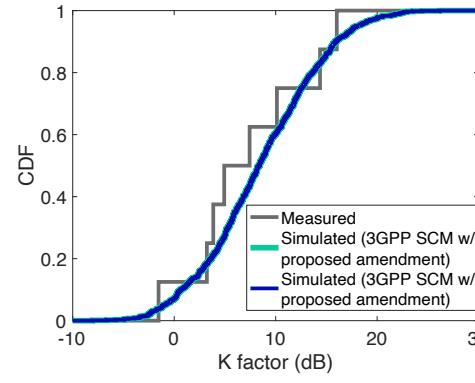

FIGURE 21. **K factor distribution.**

in terms of the distribution of these variables. Fig. 18 shows the distribution of the delay spread calculated from the measured PADP and from the generated channel responses. Both the proposed channel generation procedure and the baseline procedure generate responses consistent with the measurement. Note that the characteristics of the delay spread distribution from the proposed and baseline procedures are almost identical. This is because we did not amend the generation method of the cluster excess delay $\tau_1, \ldots, \tau_N$ and cluster power $P_1, \ldots, P_N$, which are the main factors determining the behavior of the delay spread distribution.

Fig. 19 shows the distribution of the azimuth AoA spread calculated from the measured PADP and the generated channel responses. Comparing the proposed procedure with the baseline, the azimuth AoA in the proposed procedure distributes in slightly larger values than the baseline procedure. This is because of the amendment in the generation method of the cluster azimuth AoA. In the proposed procedure, the cluster azimuth AoAs are generated with a uniform distribution where a cluster with a larger power can distribute uniformly within the range of the uniform distribution in the azimuth AoA. Hence, the channel samples with a larger azimuth AoA spread can be yielded. In the baseline, this effect does not occur because this baseline applies a wrapped Gaussian distribution, where the generated power angular profile exhibits a Gaussian shape. This implies that the cluster with a larger power cannot possess a larger azimuth AoA, limiting the resultant azimuth AoA spread values.

Fig. 19 may suggest that the baseline may reach a more accurate distribution in terms of the azimuth AoA spread. However, the baseline does not exhibit an accurate distribution in terms of the cluster azimuth AoA itself, which is further illustrated in Fig. 20 From this figure, we can see that the generated cluster azimuth AoA with the baseline exhibits a multimodal shape, which deviates from the measurement. Meanwhile, the proposed procedure well captures the overall statistical behavior of the cluster azimuth AoA. Hence, we can conclude that the proposed procedure reaches an accurate generation of the azimuth AoA while retailing similar characteristics in terms of azimuth AoA spread to the measurement.

Finally, we show the K-factor distribution in Fig. 21. From this figure, we can see that the K-factor distribution of the generated channel responses with both procedures does not contradict the measurement. This is because both procedures apply the 3GPP SCM procedure, where the subpath power is manipulated to retain the K-factor value as the target value generated in the first step in Fig. 12. Therein, the first subpath is gained by $K/(K+1)$ while the other subpaths are gained by $1/(K+1)$, where K is the generated target K-factor. This results in the K-factor retailing the exact value of K; hence, channel responses with a target K-factor can be accurately generated. Recalling that this target K-factor is generated with the fitted model to the measurement, the resultant K-factor

distribution does not deviate from the measurement for both procedures.

VI. CONCLUSIONS

This study holistically derived statistical channel propagation characteristics at an unexplored 95 GHz band for a conference room short-range communication use case via a propagation measurement. This investigation revealed that the delay spread ranged from 3 ns to 10 ns at most, the azimuth AoA spread ranged from 10° to 40°at most, and the K-factor ranged from 0 dB to 20 dB at most, approximately. Moreover, the path loss model was also derived, where the path loss exponent was 1.74, and the standard deviation of the power dispersion from the path loss model was 0.83 dB. These characteristics are shown to be mostly close to the 60 GHz band measurement at a similar environment rather than the 3GPP indoor office environment at 95 GHz. Hence, the frequency difference between the 60 GHz and 95 GHz bands is not a major factor affecting the statistical characteristics, and for a large-scale channel characterization, these two bands can be jointly modeled when the same environment is considered at least for this small room short-range communication environment.

Moreover, for the generation of detailed channel responses, we proposed an essential amendment for the 3GPP SCM to accurately re-generate intra-cluster channel characteristics for the usage of a large bandwidth. The key idea was an unequal generation of intra-cluster subpath characteristics, where the number of clusters, per-cluster delay spread, and per-cluster azimuth AoA spread are forced to be different from cluster to cluster. Via numerical evaluations, this amendment was shown to reach a closer trend of intra-cluster characteristics in terms of the number of clusters, per-cluster delay spread, and per-cluster azimuth AoA spread. This proposed amendment enhanced the channel generation performance in terms of the intra-cluster characteristics retailing the benefit of 3GPP SCM where the overall delay spread, azimuth AoA spread, and K-factor are consistent to the measurement.

This study left several future works. Based on our propagation measurement, we may hypothesize that the statistical channel parameters in the 60 GHz and 95 GHz can be unified not only for the small room short-range communication scenario but also for other scenarios. This hypothesis should be confirmed via an extensive channel measurement for various environments. Moreover, extending the proposed amendment to the system level by considering the spatial correlation may be an interesting research direction.

REFERENCES

[1] Y. Koda, N. Ohmi, H. Endo, and H. Harada, "95 GHz sub-THz multipath propagation measurement for indoor conference room desktop," *in Proc. IEEE WCNC 2024*, Dubai, UAE, Apr. 2024, pp. 1–6.

[2] M. A. Uusitalo *et al*., "6G vision, value, use cases and technologies from European 6G flagship project Hexa-X," *IEEE Access*, vol. 9, pp. 160004–160020, Nov. 2021.

[3] T. S. Rappaport *et al.*, "Millimeter wave mobile communications for 5G cellular: It will work!," *IEEE Access*, vol. 1, pp. 335–349, May 2013.

[4] T. S. Rappaport *et al.*, "Wireless communications and applications above 100 GHz: Opportunities and challenges for 6G and beyond," *IEEE Access*, vol. 7, pp. 78729–78757, Jun. 2019.

[5] 3GPP "Study on channel model for frequencies from 0.5 to 100 GHz," Tech. Report 38.901, V.17.0.0, Mar. 2022.

[6] 3GPP "Study on supporting NR from 52.6 GHz to 71 GHz," Tech. Report 38.901, V.17.0.0, Mar. 2021.

[7] "Measurement results and final mmMAGIC channel models," H2020-ICT-671650-mmMAGIC/D2.2, May 2017.

[8] H. Tsukada, K. Kumakura, S. Tang, and M. Kim, "Millimeter-wave channel model parameters for various office environments," *IEEE Access*, vol. 10, pp. 60387–60396, Jun. 2022.

[9] S. Li et al., "Measurement-based analysis and modeling of channel characteristics in an indoor-office scenario at 100 GHz," in *Proc. IEEE VTC2023-spring*, Florence, Italy, Jun. 2022, pp. 1–7.

[10] Z. Chang *et al.*, "3GPP-like THz channel modeling for indoor office and urban microcellular scenarios," *arXiv [eess.SP]*, May 2023. [Online]. Available: http://arxiv.org/abs/2305.14997

[11] [Online]. Available https://quadriga-channel-model.de/

[12] Y. Koda, R. Ouyang, N. Ohmi, and H. Harada, "Survey, taxonomy, and unification of standard mmWave channel models for WPAN, WLAN, and cellular systems in 6G," *IEEE Commun. Stan. Mag.* in Press.

[13] Y. Koda, R. Ouyang, N. Ohmi, and H. Harada, "3GPP-compatible channel generation framework for FR2-2 indoor short-range communication," *IEEE Open J. Antennas Propag.,* vol. 4, pp. 278–293, Mar. 2023.

[14] S. K. Yong, "TG3c channel modeling sub-committee final report," doc.: IEEE 15–07-0584–01-003c, Mar. 2007.

[15] 3GPP "Study on evaluation methodology of new vehicle-to-everything (V2X) use cases for LTE and NR," Tech. Report 37.885, V.15.3.0, Jun. 2019.

[16] Y. Qin *et al.*, "Time-varying channel measurement and analysis at 105 GHz in an indoor factory," in *Proc. EuCAP*, Glasgow, Scotland, Mar. 2024, pp. 1–5.

[17] X. Liu *et al.*, "Channel sparsity variation and model-based analysis on 6, 26, and 105 GHz measurements," *IEEE Trans. Veh. Technol.*, vol. 73, no. 7, pp. 9387–9397, Jun. 2024.

[18] Y. Koda, N. Ohmi, H. Endo, and H. Harada, "105 GHz multipath propagation measurements and path loss model for sub-THz indoor short-range communications," in *Proc. IEEE VTC2023-Fall,* Hong Kong, Oct. 2023, pp. 1–5.

[19] M. Maeda, Y. Koda, N. Ohmi, and H. Harada, "105 GHz indoor omnidirectional power delay profile measurement in personal office desktop environment," *to be presented at IEEE VTC 2024-fall.*

[20] M. Inomata *et al.*, "Terahertz propagation characteristics for 6G mobile communication systems," in *Proc. EuCAP*, held online, Mar. 2021, pp. 1–5.

[21] M. Inomata, W. Yamada, N. Kuno, and M. Sasaki, "Sub-terahertz propagation characteristics up to 150 GHz for 6G mobile communication systems", *International Journal of Microwave and Wireless Technologies*, vol. 15, no. 1, pp. 51–58, Apr. 2022.

[22] A. Brizzi, A. Pellegrini, L. Zhang, and Y. Hao, "Statistical path-loss model for on-body communications at 94 GHz," *IEEE Trans. Antennas Propag.*, vol. 61, no. 11, pp. 5744–5753, Nov. 2013.

[23] A. Pellegrini, A. Brizzi, L. Zhang, K. Ali, and Y. Hao, "Path loss characterization in a body-centric scenario at 94GHz," *IEICE Trans. Commun.*, vol. 96-B, pp. 2448–2454, Oct. 2013.

[24] K. Ali, A. Brizzi, A. N. Khan, and Y. Hao, "On-body NLoS radio channel at millimeter-wave frequencies," *IEEE Trans. Antennas Propag.*, vol. 71, no. 2, pp. 1783–1792, Feb. 2023.

[25] S. Ju, Y. Xing, O. Kanhere, and T. S. Rappaport, "Millimeter wave and sub-terahertz spatial statistical channel model for an indoor office building," *IEEE J. Sel. Areas Commun.*, vol. 39, no. 6, pp. 1561–1575, Jun. 2021.

[26] M. Kim, A. Ghosh, R. Takahashi, and K. Shibata, "Indoor channel measurement at 300 GHz and comparison of signal propagation with 60 GHz", *IEEE Access*, vol. 11, pp. 124040–124054, Nov. 2023.

[27] H. Poddar, S. Ju, D. Shakya, and T. S. Rappaport, "A tutorial on NYUSIM: sub-terahertz and millimeter-wave channel simulator for 5G, 6G and beyond," *IEEE Commun. Surv. Tut.*, Early Access, Dec. 2023.

[28] C. Han *et al.*, "Terahertz wireless channels: A holistic survey on measurement, modeling, and analysis," *IEEE Commun. Surv. Tut.*, vol. 24, no. 3, pp. 1670–1707, thirdquarter 2022.

[29] [Online]. Available: https://www.keysight.com/jp/ja/assets/7018-05100/configuration-guides/5992-1326.pdf

[30] H. Endo, Y. Koda, and H. Harada, "A time-alignment algorithm of multiple power delay profiles measured by antenna rotations towards flexible mmWave channel measurements," in *Proc. IEEE VTC2023-spring*, Florence, Italy, Jun. 2023, pp. 1–5.

[31] Y. Koda, R. Ouyang, and H. Harada, "End-to-end channel modeling and generation software based on statistical mmWave channel model," *IEEE Open J. Antennas Prop.*, vol. 4, pp. 824–839, Jul. 2023.

[32] G. R. Maccartney, T. S. Rappaport, S. Sun, and S. Deng, "Indoor office wideband millimeter-wave propagation measurements and channel models at 28 and 73 GHz for ultra-dense 5G wireless networks," *IEEE Access*, vol. 3, pp. 2388–2424, Oct. 2015.

Yusuke Koda (Member IEEE) received the B.E. degree in electrical and electronic engineering from Kyoto University in 2016, and the master's. and the Ph.D. degree in informatics from the Graduate School of Informatics, Kyoto University in 2018 and 2021, respectively, where he is currently an Assistant professor. He was a Postdoctoral Researcher with the Centre for Wireless Communications, University of Oulu, Finland in 2021, where he visited the Centre for Wireless Communications in 2019, to conduct collaborative research. His current research interest is in ultra-wideband wireless communication systems operating on mmWave/sub-THz bands and machine learning-aided wireless communication systems. Since joining 2023, he has been involved in the 3GPP standardization activities for the RAN TSG. He received the Young Researcher's Encouragement Award in 2017 from IEEE VTS Japan, the 35th Telecom System Technology Award in 2020 from the telecommunications Advancement Foundation, the 36th Telecom System Technology Student Award in 2021 from the telecommunications Advancement Foundation, Young Researcher's Encouragement Award in 2021 from the institute of electronics, information and communication engineers, Student Research Encouragement Award in 2021 from IEEE Kansai Chapter, and Outstanding Paper Award for Young C&C Researchers in 2022. He was also an IEEE Wireless Communications Letters, Exemplary Reviewer in 2020. Moreover, he was a recipient of the Nokia Foundation Centennial Scholarship in 2019.

Norichika Ohmi (non-Member IEEE) received the B.E. and M.E. degrees in electrical engineering from Nagoya University, Nagoya, Japan, in 1983 and 1986, respectively. In 1986, he joined Sumitomo Electric Industries, Osaka Japan in 1986, where he was engaged in research on radio communication systems. He is currently a Researcher with Graduate School of Informatics, Kyoto University in 2022.

Hiroaki Endo (Student Member IEEE) is a candidate of an M.I. degree of Graduate School of Informatics, Kyoto University, Japan. He received a B.E. degree in Faculty of Engineering from the Kyoto University, Japan, in 2023. He received the Young Researcher's Award from IEEE VTS Tokyo/Japan Chapter in 2023.

Hiroshi Harada (Senior Member IEEE) is currently a Professor of the Graduate School of Informatics, Kyoto University, Kyoto, Japan, and a Research Executive Director of Wireless Networks Research Center, National Institute of Information and Communications Technology (NICT). He joined the Communications Research Laboratory, Ministry of Posts and Communications, in 1995 (currently, NICT). He was a Visiting Professor with the University of Electro-Communications, Tokyo, Japan, from 2005 to 2014. Since 1995, he has been researching software defined radio, cognitive radio, dynamic spectrum access network, wireless smart ubiquitous network, and broadband wireless access systems on VHF, UHF, microwave, and millimeter-wave bands. In 2014 he was a Professor of Kyoto University. He has authored the book entitled Simulation and Software Radio for Mobile Communications (Artech House, 2002). He has also joined many standardization committees and forums in the United States and also in Japan and fulfilled important roles for them, especially IEEE 1900 and IEEE 802. He was the Chair of IEEE DySpan Standards Committee and the Vice Chair of IEEE 802.15.4g, IEEE 802.15.4m, 1900.4, and TIA TR-51. He was a Board of Directors of IEEE communication society standards board, SDR forum, DSA alliance, and WhiteSpace alliance. He is a cofounder of Wi-SUN alliance and was the Chairman of the board from 2012 to 2019. He is currently the Vice Chair of IEEE 2857, IEEE 802.15.4aa, IEEE 802.15.4ad and the chairman of the board, Wi-SUN alliance. He was also the final technical proponent of IEEE 802.15.3c, the world's first standard for wireless personal area networks in the millimeter waveband. He moreover was the Chair of the IEICE Technical Committee on Software Radio (TCSR) and the Chair of Public Broadband Mobile Communication Development Committee, ARIB. He is also involved in many other activities related to telecommunications. He was the recipient of the achievement awards in 2006 and 2018 and a Fellow of IEICE in 2009, respectively and the achievement awards of ARIB in 2009, 2018, and 2022, respectively, on the topic of research and development on cognitive radio and wireless smart utility network.